Applied Catalysis B: Environmental 90 (2009) 224–232

Contents lists available at ScienceDirect

Applied Catalysis B: Environmental

journal homepage: www.elsevier.com/locate/apcatb

Morphology effects of nanoscale ceria on the activity of Au/CeO_2 catalysts for low-temperature CO oxidation

Xin-Song Huang, Hao Sun, Lu-Cun Wang, Yong-Mei Liu *, Kang-Nian Fan, Yong Cao *

Shanghai Key Laboratory of Molecular Catalysis and Innovative Materials, Department of Chemistry, Fudan University, Shanghai 200433, PR China

ARTICLE INFO

Article history:
Received 7 January 2009
Received in revised form 22 February 2009
Accepted 9 March 2009
Available online 19 March 2009

Keywords:
Gold
Ceria
Low-temperature oxidation of CO
Morphology effect

ABSTRACT

Catalytic properties of Au nanoclusters deposited on a one-dimensional CeO_2 (1-D) nanorod and CeO_2-nanoparticles have been investigated during CO oxidation at ambient temperatures. The kinetic data showed that the activity of Au catalysts could be remarkably improved by using CeO_2-nanorods as support compared to the CeO_2-nanoparticles. The measured specific rate and apparent activation energy (E_a) at 278 K were 4.02 $mol_{CO}\ g_{Au}^{-1}\ h^{-1}$ and 15.9 kJ mol^{-1}, respectively, for the Au/CeO_2-nanorods (Au-CR) catalyst, while those for the Au/CeO_2-nanoparticles (Au-CP) catalyst were 0.15 $mol_{CO}\ g_{Au}^{-1}\ h^{-1}$ and 28.4 kJ mol^{-1}, respectively. Characterization by X-ray diffraction (XRD), transmission electron microscopy (TEM), hydrogen temperature-programmed reduction (H_2-TPR), X-ray photoelectron spectroscopy (XPS), diffuse reflectance UV–Vis spectroscopy (DR UV–Vis) and *in situ* diffuse reflectance Fourier transform infrared spectroscopy (DRIFTS) of CO adsorption reveal that the predominantly exposed {1 0 0}/{1 1 0}-dominated surface structures of ceria nanorods show great superiority for anchoring and dispersing of gold nanoclusters, which in turn leads to a higher reducibility and activity of the Au-CeO_2 surface for CO oxidation. It is also confirmed that, arising from the strong metal–support interaction (SMSI), the presence of gold nanoclusters has a strong influence on the electronic state of the CeO_2 substrates.

1. Introduction

Catalysts based on supported gold nanoparticles have attracted significant recent attention owing to their unique catalytic properties for numerous reactions [1–3], the most prominent one being the low-temperature CO oxidation [4]. It is generally agreed that the catalytic activity of gold catalysts depends critically on the size of the gold particles [5–7], but the nature of the support material, the preparation method, and the activation procedure have also been suggested to play a key role [8–14]. Exceptionally high activities for oxidation of CO have been reported for finely dispersed Au on reducible oxides, such as TiO_2, Fe_2O_3, and Co_3O_4 [6–16]. It has been proposed that the reducible metal oxide support supplies reactive oxygen (in the form of superoxide and peroxide species) to the active gold sites [4,10]. In particular, sites at the gold–support interface have been suggested to be responsible for the activity in CO oxidation [15,16]. Other factors have also been considered in the recent literature, including the charge transfer from the support, metal cation sites and low-coordinated sites [17,18]. From the point of view of an ultimate technological application of these materials, however, further improving the performance of the supported gold catalyst is still a great challenge.

Ceria has been regarded as one of the most important components in many catalytic systems due to its remarkable redox properties. Of particular interest is that CeO_2 can act as an oxygen buffer by releasing/uptaking oxygen through redox processes involving the Ce^{4+}/Ce^{3+} couple, which plays an important role in many oxidation reactions [19–21]. Nevertheless, until recently, CeO_2 is not recognized as an excellent support for gold catalyzed CO oxidation [1,2]. A notable study by Corma and his co-workers showed that greatly improved catalysts can be achieved by using a nanocrystalline form of CeO_2 (average primary crystallite size ca. 3–5 nm) [22]. These catalysts have been found to be two orders of magnitude more active than comparable catalysts prepared using a conventional CeO_2 support for room temperature CO oxidation, emphasizing the importance of the nanocrystalline nature of ceria in genesis of high activity in gold catalysis. More recent studies, however, indicate the very nature and catalytic origin of the Au-CeO_2 system is far more complex than expected previously [23,24]. Complicated redox interplay between Au clusters and CeO_2 matrix at interface has been identified [24]. In addition, the incorporation of cationic Au into ceria lattice leading to the formation of a modified $Ce_{1-x}Au_xO_{2-\delta}$ surface phase with enhanced redox activity has also been suggested [24].

* Corresponding authors. Tel.: +86 21 55665287; fax: +86 21 65643774.
E-mail addresses: ymliu@fudan.edu.cn (Y.-M. Liu), yongcao@fudan.edu.cn (Y. Cao).

0926-3373/$ – see front matter © 2009 Elsevier B.V. All rights reserved.
doi:10.1016/j.apcatb.2009.03.015

One critical issue associated with the ceria-based catalysts is the drastically improved activity or selectivity induced by strong metal–support interactions (SMSI), which depends strongly on the surface nature, i.e., morphology or exposed surface planes of the ceria supports [25–28]. In this context, there has been growing interest over the last few years in the use and the origin of the shape-dependent or structure sensitive behavior of the ceria systems [29–42]. One remarkable example is that single crystalline CeO_2 with 1D-like morphology predominantly exposing their {1 0 0} and {1 1 0} planes were found to be far more reactive than polycrystalline CeO_2 powders in CO oxidation [29]. Subsequent DFT theoretical calculations have revealed that the less compact {1 0 0} and {1 1 0} planes are more reactive with respect to {1 1 1} facet in terms of CO adsorption and activation [38,39]. Several recent studies have confirmed that the crystal plane of ceria play an essential role in determining its catalytic oxidation properties [30–33]. Moreover, it is shown that the favorable synergistic interaction between CuO and the more reactive {0 0 1} and {1 1 0} planes of CeO_2-nanorods can lead to significantly enhanced activity for CO oxidation [36]. Most recently, a strong shape/crystal plane effect of CeO_2 on the gold-ceria activity for water–gas shift (WGS) reaction has been also demonstrated [37].

To the best of our knowledge, very little is known for Au-CeO_2-nanocomposites with respect to the surface structural effect of CeO_2 on the redox interplay between Au and CeO_2 for CO oxidation. To clarify the possible morphology or shape effects of nanoscale ceria on the redox activity of Au/CeO_2 catalysts, we synthesized a one-dimensional CeO_2-nanorod and deposited Au species on its surface. The catalytic activity of the Au/CeO_2-nanorod is examined in CO oxidation under mild conditions. The remarkable improvement of the activity for Au/CeO_2-nanorod relative to a conventional nanoparticle CeO_2 supported Au has been elucidated in accordance with a preliminary studies of X-ray diffraction (XRD), transmission electron microscopy (TEM), diffuse reflectance UV–Vis spectroscopy (DR UV–Vis), *in situ* infrared spectroscopy (IR) coupled with CO adsorption, temperature-programmed reduction (H_2-TPR) and X-ray photoelectron spectroscopy (XPS).

2. Experimental

2.1. Catalyst preparation

The CeO_2-nanorods were synthesized by a modified hydrothermal method following the reported procedure [32]. Typically, $Ce(NO_3)_3{\cdot}6H_2O$ (1.5 g) was dissolved in an aqueous solution of NaOH (C_{NaOH} = 6 M), which was then transferred into a 50 mL Teflon-lined stainless steel autoclave, sealed and maintained at 373 K for 24 h. After the reaction was completed, the resulting solid product was recovered by filtration and washed thoroughly with deionized (DI) water. The final product was dried at 333 K and calcined at 673 K for 4 h.

The CeO_2-nanoparticles were prepared by a process that involves the homogeneous precipitation of a solution of cerium nitrate with a base: $Ce(NO_3)_3{\cdot}6H_2O$ was dissolved in distilled water, and then the pH value of the solution was rapidly adjusted to 10 with 10% NaOH solution with stirring. The precipitate was filtrated, washed with DI water, dried at 333 K for 24 h, and then calcined at 673 K for 4 h. The BET surface area of the pure support material is 55 and 62 $m^2\,g^{-1}$ for ceria nanorods and nanoparticles, respectively.

The deposition of Au onto the ceria substrate was conducted using a routine deposition–precipitation (DP) method originally developed by Haruta et al. [8]. In brief, the CeO_2 substrates were dispersed in an aqueous solution of $HAuCl_4$ at a fixed pH of 10. The nominal Au loading was 1.0 wt%. The suspension was aged at 333 K for 2 h and washed with DI water several times. The final Au-containing material was obtained by calcination in air 473 K for 2 h. For brevity, the 1.0 wt% Au/CeO_2-nanorods and 1.0 wt% Au/CeO_2-nanoparticle catalysts were denoted as Au-CR and Au-CP, respectively.

2.2. Characterization

The BET surface area of catalyst was obtained from the adsorption and desorption N_2 isotherms that were collected on a Micromeritics TriStar 3000 instrument at 77 K. Prior to the measurements, all samples were degassed at 573 K until a stable vacuum of ca. 5 mTorr was reached. Elemental analysis with respect to Au loading was performed using ion-coupled plasma atomic emission spectroscopy (ICP-AES) on a Thermo Electron IRIS Intrepid II XSP spectrometer. Powder X-ray diffraction data were obtained with a Bruker D8 diffractometer using Cu Kα radiation (λ = 1.540589 Å). The diffraction patterns were taken in the Bragg's angle (2θ) range from 10° to 90° at room temperature. Transmission electron microscopy images were recorded on a JEOL 2011 electron microscope operating at 200 kV. Energy dispersion spectra (EDS) were obtained from an attached Oxford Link ISIS energy-dispersive spectrometer fixed on the JEM-2011 electron microscope.

TPR measurements were carried out on a U-shape quartz reactor with a home made apparatus. Before the experiment, the samples were pretreated with a flowing gas mixture of 5% O_2 in He at atmospheric pressure, at 393 K for 1 h. The gas mixture of 5% H_2 in Ar was then left flowing on the samples with a flow rate of 40 mL min^{-1}, while heating from 293 to 1150 K at the rate of 5 K min^{-1}. XPS analysis was performed on a Perkin Elmer PHI 5000C spectrometer using Mg Kα radiation (1253.6 eV, pass energy of 20.0 eV). The carbonaceous C1 s line (284.6 eV) was used as the reference to calibrate the binding energies (BE). Diffuse Reflectance (DR) UV–Vis spectra of the solids diluted in $BaSO_4$ were recorded at room temperature on a Shimadzu UV 2450 Spectrometer equipped with an integrating sphere and using $BaSO_4$ as reference. The *in situ* DRIFT spectra were recorded using Bruker Vector 22 FT-IR spectrometer equipped with Harrick diffuse reflectance accessory and a high-temperature *in situ* cell with ZnSe windows. CO adsorption on the ceria matrix and Au catalysts were conducted in a reaction cell (modified Harrick model HV-DR2) to allow gas to flow continuously through the catalyst bed (ca. 0.02 g) during spectra acquisition. Contributions from gas-phase CO were eliminated by subtracting the corresponding spectra from the pure KBr powder.

2.3. Activity measurements

The catalytic activity tests were performed at atmospheric pressure in a quartz tube micro reactor (i.d. 3 mm). The catalyst weight was 20 mg, and the total flow rate of the reaction gas was 37 mL min^{-1}, with a composition of 1%CO–20%O_2 (balanced with He). Before reaction, the catalysts were pretreated with He (50 mL min^{-1}) at 373 K for 0.5 h. Kinetic measurements were performed under differential reaction conditions, with typically 1–2 mg catalyst powder. In order to limit the conversion to values typically between 5 and 20%, the catalyst samples were diluted with chemically inert α-Al_2O_3. Reactions were carried out with a flux of 100 mL min^{-1} at 298 K in CO and O_2 and He as balance. Kinetic data were acquired after 60 min reaction time. The composition of the influent and effluent gas was detected with an online GC-17A gas chromatograph equipped with a TDX-01 column. The conversion of CO was calculated from the change in CO concentrations in the inlet and outlet gases.

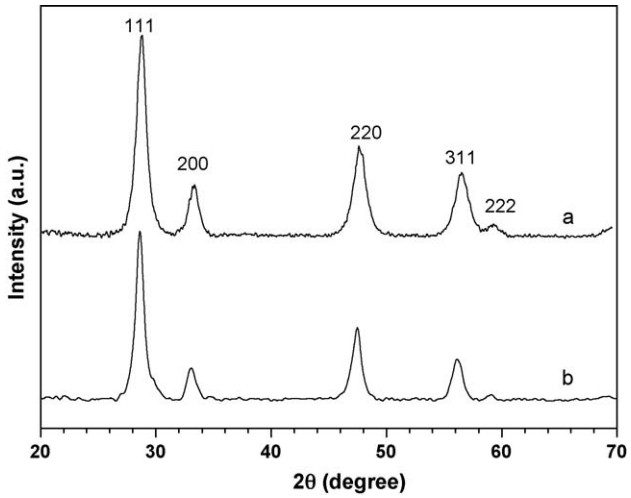

Fig. 1. XRD patterns of (a) Au-CR and (b) Au-CP.

3. Results and discussion

3.1. Catalysts characterization: XRD, TEM and TPR

The XRD patterns (Fig. 1) of the two as-synthesized Au-CeO_2 catalysts show only the face-centered cubic (fcc) structure of CeO_2 (a = 5.411 Å, space group: $Fm3m$) without any Au phase. The TEM images in Fig. 2 show that the two differently shaped ceria nanoparticles maintain their original crystal shapes after gold deposition—the CeO_2-nanorods display a uniform width of (15 ± 2.8) nm with a length of 80–100 nm (Fig. 2a), and the CeO_2-nanoparticles have a diameter of (8.0 ± 2.1) nm (Fig. 2c, Table 2). A typical HRTEM image combined with a fast Fourier transform (FFT) analysis was provided in Fig. 2b. A recent TEM investigation of a similarly prepared CeO_2-nanorods by Zhou et al. [29] has revealed that the CeO_2-nanorods predominantly expose the well-defined and less stable {0 0 1} and {1 1 0} planes. On the other hand, the CeO_2-nanoparticles are dominated by a truncated octahedral shape enclosed by the {1 1 1} and {1 0 0} facets. Notably, the HRTEM data did not reveal evidence of gold particles. The high dispersion nature of the Au species was confirmed by the EDS spectra (Fig. 2e and f) of the two samples, which gave similar mean value of surface compositions (about 1 wt% Au), in good consistent with the ICP-AES results in Table 1.

The redox behavior of the ceria materials and Au-containing samples has been studied by TPR. As shown in Fig. 3 and Table 1, the TPR profile of ceria nanoparticles exhibits two reduction peaks. The low-temperature (LT) reduction peak (at ca. 750 K, 0.58 $mmol_{H_2}$ g^{-1}) is attributed to the reduction of the most easily reducible surface-capping oxygen of CeO_2 and the high-temperature (HT) peak (at ca. 1070 K, 0.85 $mmol_{H_2}$ g^{-1}) is attributed to the bulk reduction of ceria. The profile of ceria nanorods showed a similar peak of bulk reduction (at ca. 1050 K, 0.71 $mmol_{H_2}$ g^{-1}) but quite a different LT peak with much lower reduction temperature (640 K) and larger H_2 consumption (0.89 $mmol_{H_2}$ g^{-1}). Traditionally, the higher amount of hydrogen consumed in the LT reduction peak with respect to the bulk process can be related with the proportion of surface CeO_2 species in the small nanoparticles present in the support [43]. However, considering the smaller BET surface area and larger particle sizes of ceria nanorods, other critical factors must be considered in determining the TPR trace of ceria nanorods. Most likely, the higher H_2 consumption of the LT reduction peak as well as the downward shift observed for the ceria nanorods support may be associated with the easier migration of the lattice oxygen from bulk to surface on the exposed more reactive (1 0 0) and (1 1 0) planes in comparing with the ceria nanoparticle support, as suggested by Yan et al. [32].

The incorporation of gold significantly modifies the TPR profiles. The surface ceria reduction peaks at ca. 600–800 K are completely lacking, giving rise to new LT reduction peaks, centered at 372 K for Au-CR and 422 K for Au-CP, together with the bulk ceria reduction centered at 1034 K for Au-CR and 1073 K for Au-CP. The LT peak can be mainly attributed to the reduction of the surface ceria, while the reduction of the ionic gold species (estimated to be 0.01−0.02 $mmol_{H_2}$ g_{cat}^{-1}) can be neglected. Thus the different temperature shift could be viewed as an indication of the different extent of increased surface oxygen reducibility. It is known that metallic gold in analogy with other noble metals could activate the hydrogen with subsequent spillover on the support and promotion of the ceria reduction at lower temperature [44]. Venezia et al. have recently shown that a high Au dispersion can lead to a high reducibility of the ceria support [24]. It has also been suggested that the surface oxygen reducibility may be enhanced through a lattice substitution effect, i.e., the vacant Ce^{4+} sites filled with the ions Au^{+} or Au^{3+} would lead to the formation of oxygen vacancies and thus increase the oxygen mobility and reducibility [45]. Consequently, the greater easiness of H_2 reduction of Au-CR indicates the enhanced surface oxygen reducibility and higher gold dispersion.

3.2. Chemical and electronic states

The chemical states of the Au species on the catalyst surface were investigated by XPS. In Fig. 4, the XP spectrum of Au 4f for Au-CR showed strongly broadened peaks, with the FWHMs around 2.7 eV, suggesting a contribution of Au species with varying electronic states. After the Au 4f curve fitting, the spectrum consists of a pair of distinct peaks at 83.8 and 87.5 eV, which are typical of metallic Au^0 species [46]. The additional shoulders at 85.5 and 89.2 eV with a BE shift of +1.7 eV in the latter doublet, close to that reported for small metallic clusters or oxidized surface gold species, represents an oxidation state close to Au^{+}, possibly $Au^{\delta+}$ species [47]. Such two doublets also exists in the Au-CP sample, with the fraction of $Au^{\delta+}$ being much smaller, as indicated by the weaker shoulder as well as the fitting results reported in

Table 1
Au loading, reduction peak position, H_2 consumption, surface composition, and band gaps of various samples.

Catalyst	Au loading[a] (wt%)	Peak position[b] (K)		H_2 consumption (mmol/g)		Surface content of $Au^{\sigma+}$ (%)[c]	Surface content of Ce^{3+} (%)[c]	Band gap (eV)
		T_1	T_2	n_1	n_2			
Au-CR	0.98%	372	1034	1.05	0.68	29	30	2.65
Au-CP	0.94%	422	1073	0.97	0.80	14	32	2.37
CR	-	640	1070	0.89	0.71	-	18	2.77
CP	-	756	1073	0.58	0.85	-	25	2.70

[a] Determined by ICP-AES analysis.
[b] The temperature at the maximum of the main reduction peak in the TPR profiles.
[c] Determined by XPS curve fitting.

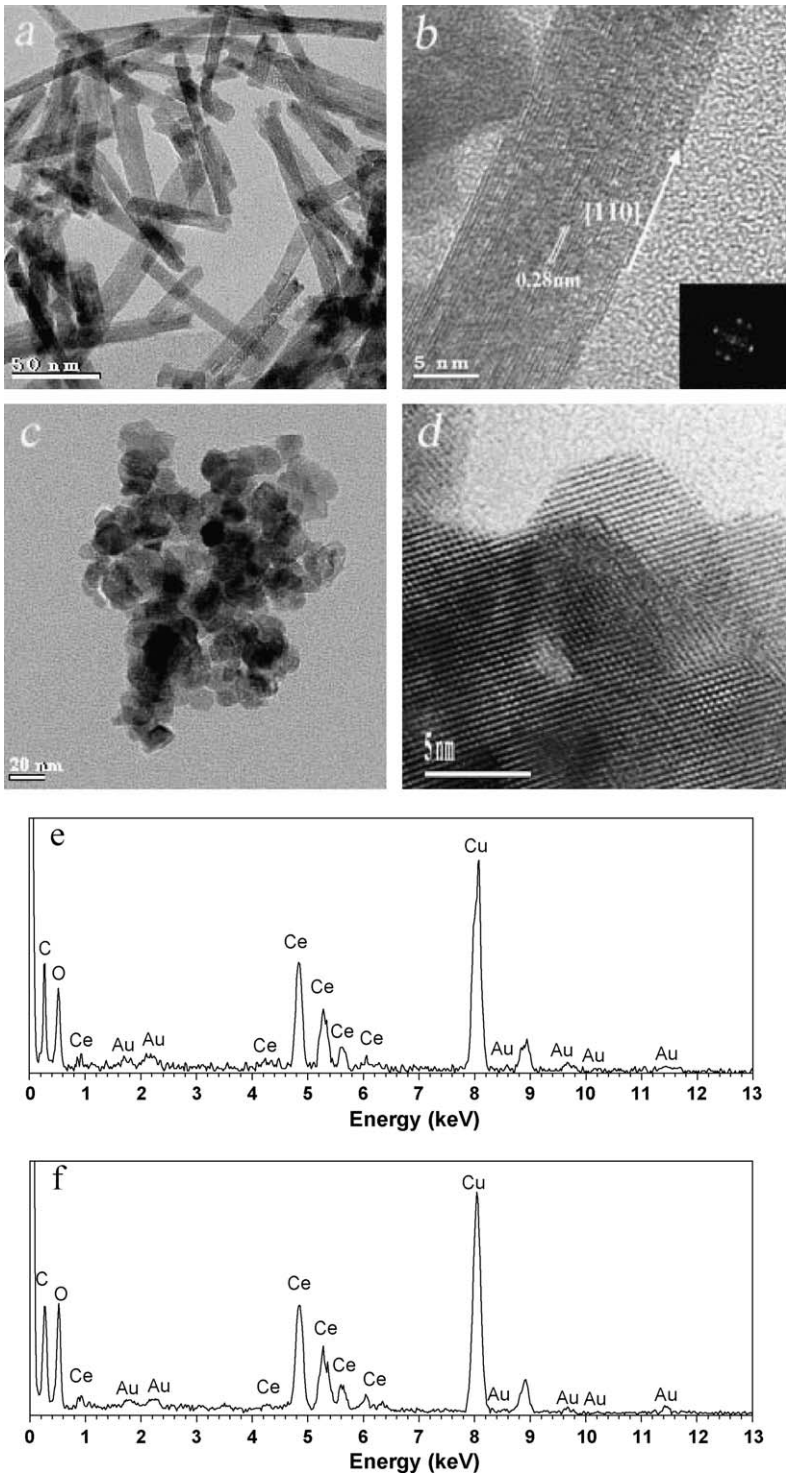

Fig. 2. Representative TEM images and EDS analysis of Au-CR (a, b, e) and Au-CP (c, d, f). The inset in figure b is the Fourier transform of individual domains in the HRTEM images.

Table 1. It has been reported that rare earth oxide supports like ceria can efficiently stabilize the oxidized gold species, such as AuO^- [48,49]. The properties of the finely dispersed gold clusters were found to be greatly influenced by the shape or crystal plane structure of the ceria supports and a direct influence of CeO_2 on the electronic states of anchored gold species has been reported [46]. Hence, the higher fraction of $Au^{\delta+}$ species in Au-CR sample may arise from the well-defined surface structures, especially the dominant {1 1 0} directed facets.

The complex XP spectra of Ce (3*d*) region of the supports before and after gold loading are evaluated by the method introduced by Hilaire et al. [50]. As shown in Fig. 5, 10 peaks are identified: 2 doublets resulting from Ce_2O_3 (dashed lines) and 3 doublets from CeO_2 (solid lines). The content of Ce^{3+} compiled in Table 1 is derived from the ratio of the integral intensities of dashed lines to the five doublets [51,52]. Further details on the evaluation of ceria XP spectra have been given in the above-cited references. The deconvolution results agreed well with the broad literature

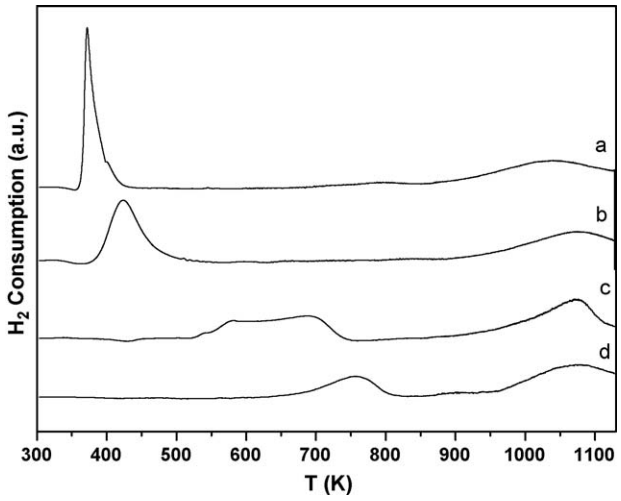

Fig. 3. H_2-TPR profiles of: (a) Au-CR, (b) Au-CP, (c) CR, (d) CP.

[24,53,54]. The amount of Ce^{3+} detected in the CR sample is about half of that for CP, possibly due to the higher surface crystallinity of CR. However, the deposition of gold increases the Ce^{3+} contribution on CR to a larger extent, i.e., ca. 12% for Au-CR and 7% for Au-CP. A similar gold-induced modification of ceria has been reported and evidenced by IR study where cerium is reduced to Ce^{3+} along with the formation of uncoordinated sites near the very small gold clusters with $d \leq 1$ nm [55]. Thus it can be suggested that for Au-CR, the higher fraction of Ce^{3+} species increased by gold (ΔCe^{3+}) indicates a stronger gold-induced modification of the surface properties of CR.

Additional information on the surface electronic states can be obtained from UV–Vis diffuse reflectance measurements. The UV–Vis spectra of various samples are presented in Fig. 6. The spectra of CR and CP (a and c) exhibited an intense absorption band with maximum at about 307 nm. According to the literature, the bands at 278 and 313 nm for pure CeO_2 can be ascribed to the overlapping of the $Ce^{4+} \leftarrow O^{2-}$ charge transfer and interband transitions, respectively [56,57]. The introduction of gold induced a slight shift of the maximum to higher wavelength. This can be explained as an introduction of energy levels in the interband gap, implying a decrease in the band gap of the ceria material when doping with transition metal ions [58,59]. By plotting the square root of the Kubelka-Munk function multiplied by the photo energy versus the photon energy and extrapolating the linear part of the rising curve to zero [60–62], the band gaps of the materials can be estimated. As depicted in Table 1, the band gap was 2.65 and 2.37 eV for Au-CR and Au-CP, respectively. It has been reported that the catalytic activity of CeO_2-based materials increases proportionally with the band gap [63]. Higher catalytic activity could be obtained when the energy levels are closer to the ones of O^{2-} (3.1 eV), since the electron transfer between oxygen atoms of ceria and gold is easier. The higher band gap of Au-CR also indicates a better synergic effect between gold and the support due to stronger interaction. In addition to the charge-transfer bands due to CeO_2, the UV–Vis spectra of Au-containing samples present a weak and wide band in the region 450–700 nm which does not appear for the pure supports. This band is due to the surface plasmon resonance of the metallic Au nanoparticles and is affected by the morphology of gold particles and the dielectric properties of the chemical environment [64]. The Au-CR catalyst exhibits a band with smaller wavelength and weaker wave strength compared to Au-CP, indicating smaller particle sizes with better Au dispersion.

Note that both the XPS and UV–Vis characterization were performed under *ex situ* conditions and a direct correlation between chemical states and active sites is not valid. Therefore, *in situ* DRIFT was used to study the adsorption of CO under simulated reaction conditions (1%CO/20%O_2/He) at RT to gain further insight into the nature of the exposed Au sites. As shown in

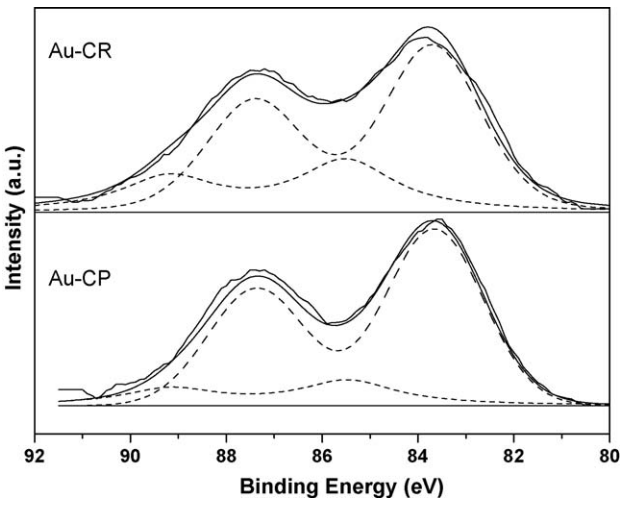

Fig. 4. Au 4f XPS spectra of (a) Au-CR and (b) Au-CP.

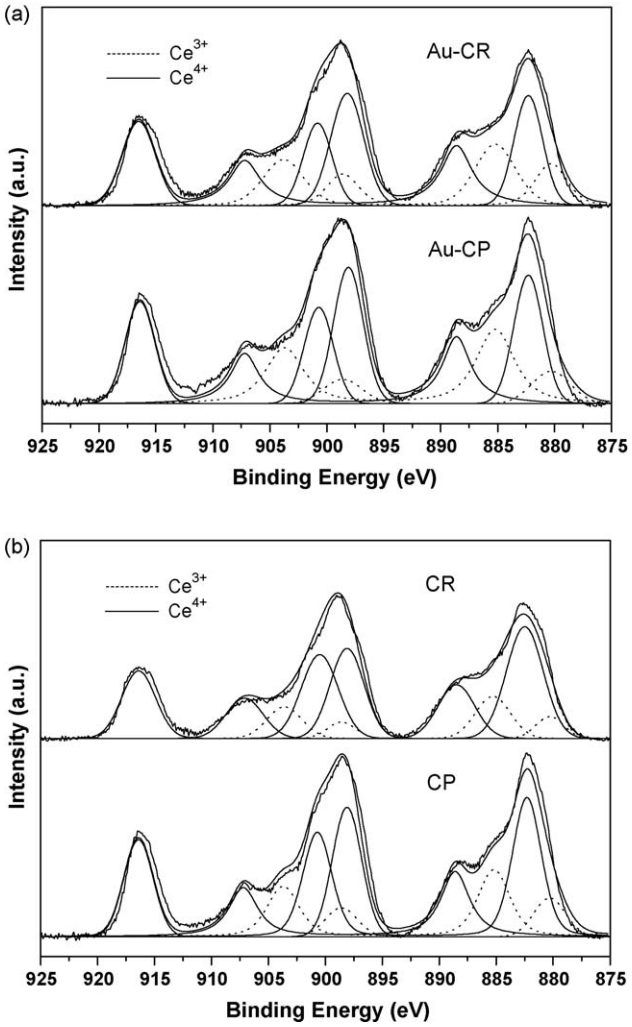

Fig. 5. (a) XPS spectra of the Ce(3d) region of Au-CR and Au-CP. (b) XPS spectra of the Ce(3d) region of CR and CP.

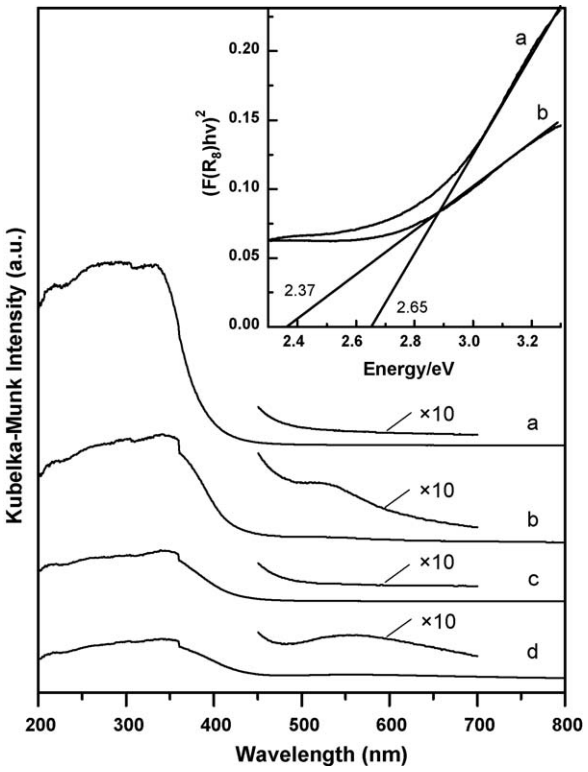

Fig. 6. DR UV–Vis spectra of (a) CR, (b) Au-CR, (c) CP, (d) Au-CP. Inset presents plots of the square root of the Kubelka-Munk function multiplied by the photon energy *vs* the photon energy of (a) Au-CR, (b) Au-CP.

Fig. 7, both Au-CR and Au-CP samples exhibited an asymmetry peak related to CO adsorption (2050–2150 cm^{-1}), which indicates the presence of gold species with different chemical states. Also notable are the prominent bands at 2361 and 2340 cm^{-1}, which are associated with CO_2 in the gas phase produced by the oxidation of CO, indicating that both catalysts are active at RT. The main peak at 2114 cm^{-1} is assigned to CO on the low-coordination sites of metallic gold particles (CO-Au^0) [65]. The shoulder band at 2127 cm^{-1} could be related to CO co-adsorbed with oxygen species on gold sites in close contact with the support [55]. One may argue that the band at 2127 cm^{-1} might be related to the electronic transition related to Ce^{3+}, however, such assignment

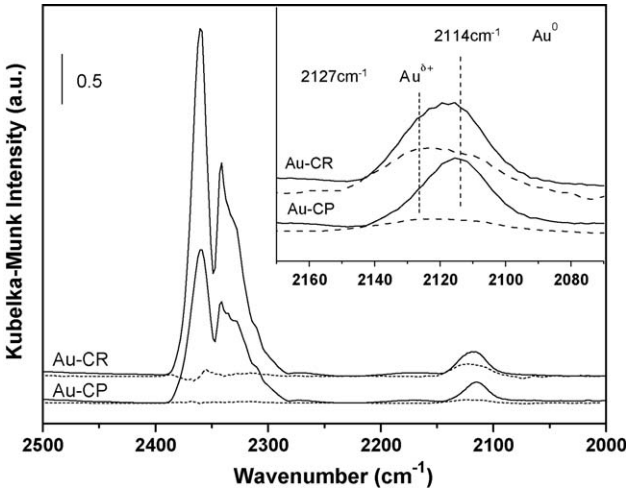

Fig. 7. DRIFT spectra of Au-CR and Au-CP after CO adsorption for 60 min under 1%CO/20%O_2/He at 298 K (solid line), after outgassing at 298 K for 30 min (dash line). Inset shows the spectra in the range 2170–2070 cm^{-1}.

is not applicable for Au/CeO_2 sample in the present work since the spectra were collected under an oxygen-rich environment. Similar conclusion has also been reached by Tabakova et al. [55]. Moreover, we did not detect such a band on the pure ceria sample (spectra not shown) even after reduction pretreatment at 200 °C. The spectra were also collected after evacuation for 30 min subsequent to the CO + O_2 adsorption, as shown in Fig. 7. It can be seen that the intensity of the band at 2114 cm^{-1} declined more rapidly than that of the band at 2127 cm^{-1}, indicating better stability of the latter band. It is known that the interaction between CO and positive Au clusters is stronger than that related to CO on reduced gold [66]. Therefore, this fact further confirms the assignment proposed. Furthermore, it can be clearly seen that the asymmetric broadening from the high-frequency side is significantly stronger for Au-CR sample, indicating the presence of higher amount of positive gold species. This finding is in good agreement with the XPS results and strongly suggests that the interaction between gold and the ceria support is stronger in Au-CR sample.

3.3. Catalytic CO oxidation

The catalytic performances of the Au-CeO_2 catalysts in CO oxidation are shown in Fig. 8a, where the CO conversion is reported

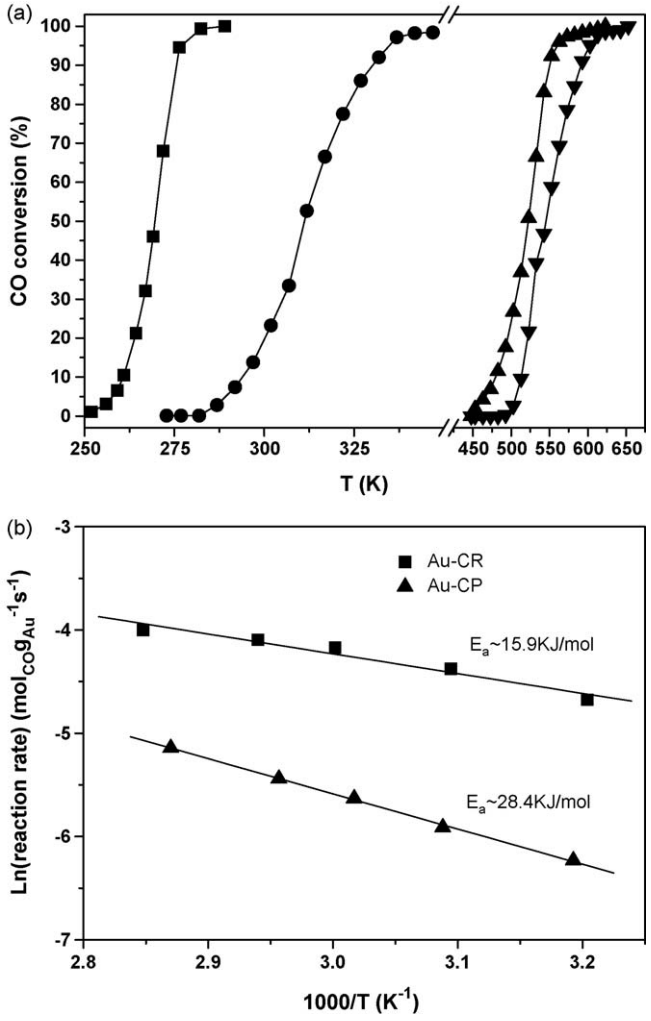

Fig. 8. (a) CO oxidation activity of (■) Au-CR, (●) Au-CP, (▲) CR, and (▼) CP. Reaction conditions: 20 mg catalyst for Au-CR and Au-CP, 50 mg catalyst for CR and CP, 1%CO–20%O_2 balanced with He, 37 mL min^{-1}. (b) Arrhenius plots of the reaction rate ln(*r*) *vs* 1/*T* for CO oxidation over (■) Au-CR and (▲) Au-CP catalysts.

as a function of temperature (light-off test). For comparison, the activities of the parent cerium oxides are also included. It is clear that the activities of the Au-containing catalysts are markedly higher than those for the corresponding parent support materials. The data in Fig. 8a also indicate that the CO oxidation activity of CeO_2-nanorods is much higher than that for CeO_2-nanoparticles, which is in good agreement with the literature results measured under similar conditions [22,24,33,34]. The temperature at which the conversion was 50% ($T_{1/2}$) for CR is 523 K, which is 250 K higher than that for Au-CR. Moreover, one can see that complete oxidation of CO could be attained at sub-ambient temperature over Au-CR. At 278 K, the rate of CO oxidation over Au-CR was 4.02 $mol_{CO}\ g_{Au}^{-1}\ h^{-1}$, about 26 times higher that for Au-CP (0.15 $mol_{CO}\ g_{Au}^{-1}\ h^{-1}$). Another notable issue from Fig. 1a is the smooth light-off behavior for CeO_2-nanorod supported Au catalyst, in contrast to that on Au-CeO_2-nanoparticles. Likely, the physical structure of the CeO_2-nanorod support is advantageous in avoiding diffusion or mass-transfer limitation.

Fig. 8b presents the reaction rates (r_{Au}) that are normalized to gold mass for these catalyst samples plotted against the reciprocal of the temperature. Notably, Au-CR shows much lower apparent activation energy (E_a) as compared to Au-CP (15.9 kJ mol^{-1} *vs* 28.4 kJ mol^{-1}). Presumably, this can be attributed to the dramatically different synergistic redox interplay between gold and CeO_2 as described above. Moreover, it is seen that the reaction rate is governed by the pre-exponential term ln *A*, inferring the presence of a higher population of the active centers in the higher loaded samples. Here it is also interesting to make a further comparison of the catalytic performance of the Au-CR catalyst with other reported CeO_2-based Au catalysts in the oxidation of CO. It is known that the activities of gold catalysts can be greatly influenced by gold particle size, the nature of support and reaction conditions [2,67]. Therefore, a straightforward comparison of activities for different catalytic systems is usually difficult. However, there are general agreements that small gold particle size is indispensable for its high activity and that synergistic redox interplay between gold and the reducible support is of vital importance for attaining high oxidation activity [1–4,8–12]. These conclusions can also be corroborated by the data listed in Table 2. A rough comparison of the mass-specific reaction rate with other Au-CeO_2 catalysts under similar reaction conditions reveals that the present Au-CR catalyst appears to be among the most active ceria-based gold catalysts reported thus far.

To clarify the essential role of ceria, particularly with respect to its oxygen activation capability for CO oxidation, the activity tests using different stream compositions were performed. Fig. 9 compares the temperatures at which the CO conversion over Au-CeO_2 catalysts reached 10% and 50% (T_{10}, T_{50}) as a function of the gas mixtures composition (CO/O_2 ratio). Presumably, if the activity is controlled by O_2 activation, one would expect a decrease in activity when the reaction is carried out in O_2-lean gas mixtures. Indeed, a decrease in O_2 concentration in gas mixture leading to a pronounced increase in temperature at which 10 and 50% CO conversion has been observed for Au-CP. Nevertheless, no appreciable difference in the T_{10} and T_{50} values is identified for Au-CR. Note that this feature may be of particular interest for some practical applications. The ability to preserve high activity in both stoichiometric and O_2-lean gas mixtures suggests participation of the CeO_2-nanorod support in the CO oxidation not only in providing centers for oxygen activation but also as a more efficient buffer in releasing–uptaking oxygen through the redox processes realized by Ce^{4+}/Ce^{3+} redox couple.

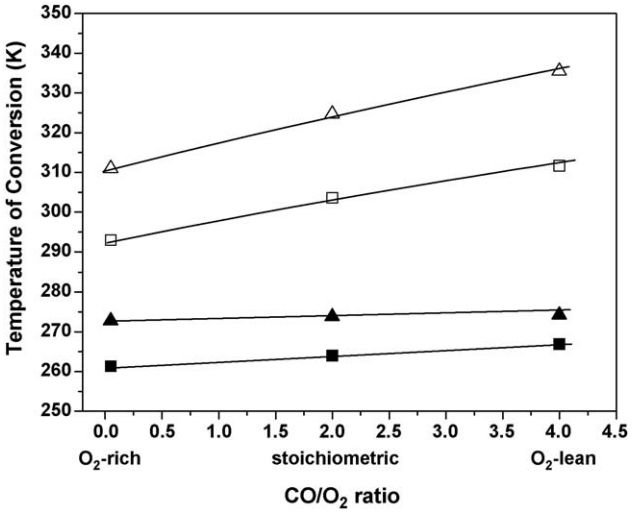

Fig. 9. T_{10} (■, □) and T_{50} (▲, △) *vs* CO/O_2 ratio over Au-CR (filled symbols) and Au-CP (open symbols). O_2-rich, $CO:O_2:He$ = 1:20:79 vol.%; stoichiometric, $CO:O_2:He$ = 1:0.5:98.5 vol.%; O_2-lean, $CO:O_2:He$ = 1:0.25:98.75 vol.%; W/F = 0.32 g s cm^{-3}.

3.4. Discussion

The results in this study indicate that the specific surface structure of ceria plays an important role in determining the chemisorptive and redox properties of the Au-CeO_2 system. Although influence of the structure or morphology of ceria has been observed previously for Au-CeO_2 in low-temperature CO oxidation [22–24,33,35], in most cases the nanocrystalline nature or crystallite size of the ceria support has been considered the key parameter that determines the synergistic redox interplay between gold and CeO_2 [22]. Based on the results of the present work, it follows that not the crystallite size, but rather surface structure, more specifically the exposed surface planes of the crystalline CeO_2 support, is important for achieving a high redox and catalytic activity of ceria supported Au material.

To explain the enhanced activity of the Au-CeO_2-nanorod catalysts, at least two factors should be considered. First, the creation and stabilization of the "catalytically active" gold may depend on the crystallographic orientation of ceria surface. Compared to other oxides, perhaps the most important property of ceria in catalysis is the readiness of the formation of oxygen vacancies, which is believed to play an important role in many

Table 2
Comparison of published literature data for CO oxidation rates on ceria supported Au catalysts with data obtained in this work.

Catalyst	Preparation	d_{Ceria} (nm)	d_{Au} (nm)	W/F (g_{cat} h mol_{CO}^{-1})	Gas mixture	Temp. (K)	r_{Au} ($mol_{CO}\ g_{Au}^{-1}\ h^{-1}$)	Ref
1%Au-CR	NaOH-DP	Nanorods	n.d.	20	1% CO, 20% O2, 79%He	278	4.02	This study
1%Au-CP	NaOH-DP	8–9	n.d.	20	1% CO, 20% O2, 79%He	278	0.15	This study
2.8%Au/CeO_2	NaOH-DP	3.3	4	94	0.2% CO, 19.8% air, 80%He	278	0.38	22
3.0%Au/CeO_2	Na_2CO_3-DP	22	n.d.	37	1% CO, 1% O2, 98%He	278	0.87	24
1.5%Au/CeO_2	IMP-$NaBH_4$	Nanorods	4.5	56	1% CO balanced with air	278	0.22	33
1%Au/CeO_2	$(NH_4)_2CO_3$-DP	7–8	n.d.	111	1% CO balanced with air	278	0.18	34
3.7%Au/CeO_2	NaOH-DP	2–6	n.d.	0.05	0.5% CO in synthetic air	298	108.6	23
1%Au/CeO_2	NaOH-DP	12	2–5	0.52	3.6% CO, 21% O2, 75.4%Ar	303	176.4	35

reactions such as the oxidation of CO [19]. It is known that the formation energy of anion vacancies for different CeO_2 surfaces follows the order {1 1 0} < {1 0 0} < {1 1 1} [68]. This means that oxygen vacancies, which are indispensable for stabilizing metals, are easier to form on the CeO_2 {1 1 0} planes. Therefore, compared with ceria nanoparticles, ceria nanorods preferentially expose its {1 1 0}/{1 0 0} surfaces should be better supports for anchoring and dispersing very fine gold clusters. This would explain why gold is dispersed and stabilized more effectively on the CeO_2-nanorods, which, in turn, leads to a higher reducibility and activity of the Au-CeO_2 surface for the CO oxidation reaction.

A second aspect to explain the observed structure sensitivity is that the unique surface structure of {1 1 0} and {1 0 0} planes can significantly increase the oxygen diffusion rates through the ceria nanorods, as reflected from the experimental observation that the Au-CeO_2-nanorod catalysts can maintain its high activity even in O_2-lean reaction mixtures. Very recently, on investigating the shape effect of single crystalline CeO_2 on the redox behavior of a series of hydrothermally derived CeO_2 materials, Yan et al. disclosed that the CeO_2-nanorod is much more active for CO oxidation than CeO_2-nanopolyhedra [32]. The reason of this effect has been rationalized as the oxygen storage takes place both at the surface and in the bulk for nanorods as opposed to the pure surface-phenomena for nanoparticles. Our TPR data has confirmed that the presence of Au can lead to a further activation of the ceria nanorod, which can facilitate the migration of O-vacancies from the bulk to the ceria surface. This may well account for why the Au-CeO_2-nanorod sample can preserve its high activity even in O_2-lean conditions.

The observation that dramatically enhanced activity can be achieved for the one-dimensional structured Au-CeO_2-nanorod catalyst may provide new insight into methods of controlling the synergistic interplay between gold and CeO_2 for gold catalysis. Obviously, there is still much to learn about the nature of the interactions between ceria and gold. A recent work by Venezia et al. has emphasized the use of an already preformed ceria phase as the support for preparation of extraordinarily active Au-CeO_2 composites via a deposition–precipitation method, which show activity dramatically higher than the coprecipitation-derived materials [24]. In the present work, we have unambiguously demonstrated the unique advantage of one-dimensional structured CeO_2-nanorods as a new, promising support for the generation of novel Au-containing materials with superior redox properties for CO oxidation. Our results confirm that, by exposing more reactive surfaces of the crystalline ceria nanostructures, it is possible to design new improved ceria-based gold catalysts with enhanced redox properties.

4. Conclusions

This study demonstrates that the surface structure or morphology of ceria markedly affects the dispersion and reducibility of Au/CeO_2 catalysts. The XRD, TEM, H_2-TPR, UV–Vis, XPS and *in situ* CO adsorption results presented in this paper indicate that that the predominantly exposed {1 0 0}/{1 1 0} surface structures of ceria nanorods show great superiority for dispersing and stabilizing of Au nanoclusters, which in turn leads to a higher redox activity of the Au-CeO_2 surface for both CO and O_2 activation. As compared with the conventional CeO_2-nanoparticles supported Au catalysts, the superior activities of gold supported on CeO_2-nanorods have been attributed to the favorable creation of highly dispersed Au nanoclusters as well as the synergetic effects arising from the strong metal–support interaction between the electronically modified Au nanoclusters and the well-defined "reactive" surface of nanorods.

Acknowledgments

This work was supported by the National Natural Science Foundation of China (20633030, 20721063, 20873026, 20803012), the National Basic Research Program of China (2003CB615807), Science & Technology Commission of Shanghai Municipality (08DZ2270500, 07QH14003) and the Committee of the Shanghai Education (06SG03).

References

[1] G.C. Bond, D.T. Thompson, Catal. Rev. Sci. Eng. 41 (1999) 319.
[2] G.C. Bond, C. Louis, D.T. Thompson, Catalysis by Gold, vol. 6, Imperial College Press, London, 2006.
[3] F.Z. Su, Y.M. Liu, L.C. Wang, Y. Cao, H.Y. He, K.N. Fan, Angew. Chem. Int. Ed. 47 (2007) 334.
[4] B.K. Min, C.M. Friend, Chem. Rev. 107 (2007) 2709.
[5] M. Valden, X. Lai, D.W. Goodman, Science 281 (1998) 1647.
[6] G.R. Bamwenda, S. Tsubota, T. Nakamura, M. Haruta, Catal. Lett. 44 (1997) 83.
[7] R. Zanella, S. Giorgio, C.-H. Shin, C.R. Henry, C. Louis, J. Catal. 222 (2004) 357.
[8] M. Haruta, S. Tsubota, T. Kobayashi, H. Kageyama, M.J. Genet, B. Delmon, J. Catal. 144 (1993) 175.
[9] A. Wolf, F. Schüth, Appl. Catal. A: Gen. 226 (2002) 1.
[10] M.M. Schubert, S. Hackenberg, A.C.V. Veen, M. Muhler, V. Plzak, R.J. Behm, J. Catal. 197 (2001) 113.
[11] V. Schwartz, D.R. Mullins, W. Yan, B. Chen, S. Dai, S.H. Overbury, J. Phys. Chem. B 108 (2004) 15782.
[12] J.H. Yang, J.D. Henao, M.C. Raphulu, Y. Wang, T. Caputo, A.J. Groszek, M.C. Kung, M. Scurrel, J.T. Miller, H.H. Kung, J. Phys. Chem. B 109 (2005) 10319.
[13] Y.F. Han, Z. Zhong, K. Ramesh, F. Chen, L. Chen, J. Phys. Chem. C 111 (2007) 3163.
[14] K. Qian, W. Huang, Z. Jiang, H. Sun, J. Catal. 248 (2007) 137.
[15] M. Haruta, Catal. Today 36 (1997) 153.
[16] M.M. Schubert, M.J. Kahlich, H.A. Gasteiger, R.J. Behm, J. Power Sources 84 (1999) 175.
[17] B. Yoon, H. Hakkinen, U. Landman, A.S. Worz, J.M. Antonietti, S. Abbet, K. Judai, U. Heiz, Science 307 (2005) 403.
[18] T. Minato, T. Susaki, S. Shiraki, H.S. Kato, M. Kawai, K.I. Aika, Surf. Sci. 566 (2004) 1012.
[19] A. Trovarelli, Catal. Rev. Sci. Eng. 38 (1996) 439.
[20] T. Bunluesin, H. Cordatos, R.J. Gorte, J. Catal. 157 (1995) 222.
[21] T. Bunluesin, R.J. Gorte, Appl. Catal. B: Environ. 15 (1998) 107.
[22] S. Carrettin, P. Concepción, A. Corma, J.M.L. Nieto, V.F. Puntes, Angew. Chem. Int. Ed. 43 (2004) 2538.
[23] Z. Tang, J.K. Edwards, J.K. Bartley, S.H. Taylor, A.F. Carley, A.A. Herzing, C.J. Kiely, G.J. Hutchings, J. Catal. 249 (2007) 218.
[24] A.M. Venezia, G. Pantaleo, A. Longo, G.D. Carlo, M.P. Casaletto, F.L. Liotta, G. Deganello, J. Phys. Chem. B 109 (2005) 2821.
[25] M. Abid, V. Paul-Boncour, R. Touroude, Appl. Catal. A: Gen. 297 (2006) 48.
[26] N. Tsubaki, K. Fujimoto, Top. Catal. 22 (2003) 325.
[27] J. Silvestre-Albero, F. Rodriguez-Reinoso, A. Sepulveda-Escribano, J. Catal. 210 (2002) 127.
[28] L. Fan, K. Fujimoto, J. Catal. 172 (1997) 238.
[29] K. Zhou, X. Wang, X. Sun, Q. Peng, Y. Li, J. Catal. 229 (2005) 206.
[30] M. Nolan, G.W. Watson, J. Phys. Chem. B 110 (2006) 16600.
[31] E. Aneggi, J. Llorca, M. Boaro, A. Trovarelli, J. Catal. 234 (2005) 88.
[32] H.X. Mai, L.D. Sun, Y.W. Zhang, R. Si, W. Feng, H.P. Zhang, H.C. Liu, C.H. Yan, J. Phys. Chem. B 109 (2005) 24380.
[33] P.X. Huang, F. Wu, B.L. Zhu, X.P. Gao, H.Y. Zhu, T.Y. Yan, W.P. Huang, S.H. Wu, D.Y. Song, J. Phys. Chem. B 109 (2005) 19169.
[34] X.Y. Wang, S.P. Wang, S.-R. Wang, Y.Q. Zhao, J. Huang, S.M. Zhang, W.P. Huang, S.-H. Wu, Catal. Lett. 112 (2006) 115.
[35] U.R. Pillai, S. Deevi, Appl. Catal. A: Gen. 299 (2006) 266.
[36] B. Skårman, L.R. Wallenberg, P. Larsson, A. Andersson, J. Bovin, S.N. Jacobsen, U. Helmersson, J. Catal. 181 (1999) 6.
[37] R. Si, M. Flytzani-Stephanopoulos, Angew. Chem. Int. Ed. 47 (2008) 1.
[38] D.C. Sayle, S.A. Maicaneanu, G.W. Watson, J. Am. Chem. Soc. 124 (2002) 11429.
[39] Z. Yang, T.K. Woo, K. Hermansson, Chem. Phys. Lett. 396 (2004) 384.
[40] I. Dobrosz-Gómez, I. Kocemba, J.M. Rynkowski, Appl. Catal. B: Environ. 83 (2008) 240.
[41] I. Dobrosz-Gómez, I. Kocemba, J.M. Rynkowski, Appl. Catal. B: Environ., doi:10.1016/j.apcatb.2008.09.028, in press.
[42] I. Dobrosz-Gómez, I. Kocemba, J.M. Rynkowski, Catal. Lett. 128 (2008) 297.
[43] A. Sepúlveda-Escribano, F. Coloma, F. Rodriguez-Reinoso, J. Catal. 178 (1998) 649.
[44] F. Boccuzzi, A. Chiorino, M. Manzoli, D. Andreeva, T. Tabakova, J. Catal. 188 (1999) 176.
[45] Q. Fu, H. Saltsburg, M. Flytzani-Stephanopoulos, Science 301 (2003) 935.
[46] E.D. Park, J.S. Lee, J. Catal. 186 (1999) 1.
[47] J.F. Moulder, W.F. Stickle, P.E. Sobol, K.D. Bomben, in: J. Chastain, R.C. King, Jr. (Eds.), Handbook of X-Ray Photoelectron Spectroscopy, Physical Electronics, Eden Prairie, MN, 1995.
[48] A.N. Pestryakov, V.V. Lunin, A.N. Kharlanov, D.I. Kochubey, N. Bogdanchikova, A.Y. Stakheev, J. Mol. Struct. 642 (2002) 129.
[49] A.N. Pestryakov, V.V. Lunin, J. Mol. Catal. A: Chem. 158 (2000) 325.

[50] S. Hilaire, X. Wang, T. Luo, R.J. Gorte, J. Wagner, Appl. Catal. A: Gen. 215 (2001) 271.
[51] M. Romeo, K. Bak, J. El Fallah, F. Le Normand, L. Hilaire, Surf. Interface Anal. 20 (1993) 508.
[52] F. Zhang, P. Wang, J. Koberstein, S. Khalid, S.W. Chan, Surf. Sci. 563 (2004) 74.
[53] R. Leppelt, B. Schumacher, V. Plzak, M. Kinne, R.J. Behm, J. Catal. 244 (2006) 137.
[54] A. Karpenko, R. Leppelt, J. Cai, V. Plzak, A. Chuvilin, U. Kaiser, R.J. Behm, J. Catal. 250 (2007) 139.
[55] T. Tabakova, F. Boccuzzi, M. Manzoli, D. Andreeva, Appl. Catal. A: Gen. 252 (2003) 385.
[56] M.I. Zaki, G.A.M. Hussein, S.A.A. Manssur, H.M. Ismael, G.A.H. Mekhemer, Colloids Surf. A 127 (1997) 47.
[57] A. Bensalem, J.C. Muller, F. Bozon-Verduraz, J. Chem. Soc. Faraday Trans. 88 (1992) 153.
[58] J.A. Navio, M.C. Hidalgo, G. Colón, S.G. Botta, M.I. Litter, Langmuir 17 (2001) 202.
[59] G.R. Rao, H.R. Sahu, Proc. Indian Acad. Sci. (Chem. Sci.) 113 (2001) 651.
[60] S.P. Tandom, J.P. Gupta, Phys. Status Solidi 38 (1970) 363.
[61] R.S. Weber, J. Catal. 151 (1995) 470.
[62] D.G. Barton, M. Shtein, R.D. Wilson, S.L. Soled, E. Iglesia, J. Phys. Chem. B 103 (1999) 630.
[63] M.À. Centeno, C. Portales, I. Carrizosa, J.A. Odriozola, Catal. Lett. 102 (2005) 289.
[64] P. Mulvaey, Langmuir 12 (1996) 788.
[65] M. Mihaylov, H. Knözinger, K. Hadjiivanov, B.C. Gates, Chem. Ing. Tech. 79 (2007) 795.
[66] M. Manzoli, F. Boccuzzi, A. Chiorino, F. Vindigni, W. Deng, M. Flytzani-Stephanopoulos, J. Catal. 245 (2007) 308.
[67] X. Bokhimi, R. Zanella, A. Morales, J. Phys. Chem. C 112 (2008) 12463.
[68] T.X.T. Sayle, S.C. Parker, D.C. Sayle, Phys. Chem. Chem. Phys. 7 (2005) 2936.